Journal of Thermal Science Vol.30, No.1 (2021) 100−110

https://doi.org/10.1007/s11630-020-1253-y **Article ID: 1003-2169(2021)01-0100-11**

Correlation Research between Turbulent Pressure Pulsation and Internal Sound Field Characteristics of Centrifugal Pump

CHENG Xiaorui[1,2*], WANG Peng[1], ZHANG Shuyan[1]

1. College of Energy and Power Engineering, Lanzhou University of Technology, Lanzhou 730050, China
2. Key Laboratory of Fluid Machinery and System, Gansu Provice, Lanzhou 730050, China

Abstract: In order to study the correlation between the internal flow noise of the centrifugal pump and the turbulent pressure pulsation, a single-stage single-suction centrifugal pump was used as the research object by the combination of numerical calculation and experiment. Based on the RNG k-ε model and the N-S equation, the model pump was simulated numerically by CFD. A dipole sound source was extracted by the turbulent pulse action of the volute wall surface according to the FW-H equation. The acoustic field of the model pump was solved on the basis of the boundary element method, and the sound pressure distribution of the internal flow field under the action of the dipole sound source of the volute wall and the frequency response of the inlet and outlet fields were obtained. The results show that the distribution of hydrodynamic noise inside the centrifugal pump is related to the pressure pulsation, presenting obvious dipole distribution and disturbance at the tongue. The sound pressure value of the field is mainly concentrated in the blade passing frequency and double frequency, in which the blade passing frequency is the strongest, and the sound pressure value decreases obviously under other double frequency. The main frequency of hydrodynamic noise is the blade passing frequency.

Keywords: centrifugal pump, pressure pulsation, internal sound field noise, frequency, simulation

1. Introduction

In recent years, controlling noise pollution has become an important part of protecting the environment. As a kind of important energy and fluid transport machinery, pumps are widely used in various sectors of the national economy. The noise of their operation has caused non-negligible influence on factories, communities, cabins and otherwise. It has a serious impact on people's production and life. Therefore, both the standards of military defense and civil use make the noise problem a hot research topic [1, 2].

Aiming at the study of fluid-induced hydrodynamic noise in centrifugal pumps, domestic and foreign scholars have carried out extensive analysis by theory, experiment and numerical simulation. The results show that the disturbed flow of the volute tongue and the blade and the uneven flow of the outlet are the main sources of pressure pulsation and noise [3–6]. In recent years, scholars have conducted in-depth exploration on the basis of their predecessors, summed up the internal flow law of centrifugal pumps and carried out a lot of research on the shape of their flowing parts and operating conditions [7–14].

With the rapid development of science and technology, especially the continuous improvement of numerical

Received: Apr 03, 2019 AE: DU Juan Corresponding author: CHENG Xiaorui E-mail: cxr168861@sina.com

Nomenclature

b_2	Impeller outlet width/mm	$\overline{P}$	The average pressure of the impeller rotating one week monitoring point/Pa
C_P	Pressure pulsation coefficient	Q_v	The amount of liquid delivered per unit time/$m^3 \cdot h^{-1}$
c	The speed at which sound travels in the medium/$m \cdot h^{-1}$	s_1	the acoustic monitoring points of inlet
D_1	Impeller inlet diameter/mm	s_2	the acoustic monitoring points of outlet
D_2	Impeller outlet diameter/mm	T_{ij}	Turbulent stress tensor
f_{max}	Maximum calculation frequency/Hz	u_2	Peripheral speed of the impeller outlet/$m \cdot h^{-1}$
H	Energy obtained by pumping a unit weight of fluid/m	Z	Number of blades of the impeller
L	Acoustic grid unit scale/mm	ρ	medium density/$kg \cdot m^{-3}$
N	Impeller revolutions per minute/$r \cdot min^{-1}$		

simulation, it is made possible to predict the acoustic simulation of centrifugal pumps. In this study, the internal flow field is deeply studied under the condition of excessive noise during the operation of the centrifugal pump. At the same time, the sound field of the centrifugal pump is studied by Lighthill acoustic analogy theory. The acoustics characteristics and the interaction between them are analyzed to provide a basic theory for further noise reduction [15–19].

2. Basic Equation of Sound Field Calculation

The Lighthill equation is the origin of modern aeroacoustics and the basis for studying rotating machinery noise such as centrifugal pump [20–22]. It is based on the N-S equation, combining with the continuity equation and the momentum equation. The left side of the equation is the classical acoustic wave equation, and the right side is the sound source. Its equation is as follows [20],

Continuity equation:

$$\frac{\partial}{\partial t}(\rho-\rho_0)+\frac{\partial(\rho v_i)}{\partial x_i}=0 \tag{1}$$

Momentum equation:

$$\frac{\partial(\rho v_i)}{\partial t}+\frac{\partial}{\partial x_i}\left[c_0^2(\rho-\rho_0)\right]=-\frac{\partial^2 T_{ij}}{\partial x_i} \tag{2}$$

Lighthill equation:

$$\left(\frac{\partial^2}{c_0^2\partial t^2}-\nabla^2\right)\rho=\nabla\cdot\nabla T_{ij} \tag{3}$$

In the formula: $T_{ij}=\rho\mu_i\mu_j-\tau_{ij}+\delta_{ij}\left[(P-P_0)-c_0^2(\rho-\rho_0)\right]$ is the turbulent stress tensor, where the first term is expressed as Reynolds stress and the second term is viscous stress. The third term indicates heat conduction. The Lighthill equation indicates that when the influence of the flow field on the sound wave is not considered, the classical acoustic method can be used to solve the hydrodynamic noise. According to Lighthill analogy theory, the noise source can be divided into a monopole source, a dipole source and a quadrupole source. In terms of sound power, they are the 4, 6, and 8 power of the flow velocity.

But in the actual flow field, the boundary between the fluid and the solid has a great influence on the sound propagation. Ffowcs Williams and Hawkings consider the interaction of moving objects with fluids, and introduced the FW-H equation based on Lighthill [20]. The equation is as follows:

$$\begin{aligned}\frac{\partial^2}{\partial x_i}\left[\rho' H(f)\right]-c_0^2\frac{\partial^2}{\partial x_i^2}\left[\rho' H(f)\right]=\frac{\partial}{\partial t}\left[\rho_0 V_n\delta(f)\right]-\\ \frac{\partial}{\partial x_i}\left[\left(p\delta_{ij}+\delta_{ij}\right)\frac{\partial f}{\partial x_j}\delta(f)\right]+\\ \frac{\partial^2}{\partial x_i\partial x_j}\left[T_{ij}H(f)\right]\end{aligned} \tag{4}$$

The definitions of all the variables in Eqs. (1–4) can be found in Ref. [20].

The first term on the right side of the formula represents a monopole noise source that describes the effect of the motion of the object on the volume of the fluid on the boundary. The second term on the right represents the dipole noise source, which describes the effect of the motion of the object on the surface of the fluid on the boundary. The third term on the right represents the quadrupole noise source, which describes the effect of turbulence on the source of the fluid stress, which is related to T_{ij} in the equation.

These three sources are present in the centrifugal pump at the same time. Since the medium in the pump is water, it is usually regarded as an incompressible fluid so the monopole noise source can be ignored. The fluid flow velocity in the centrifugal pump is much lower than a

Mach Number of 1.0, so the dipole noise source in the centrifugal pump is the main influencing factor. The dipole noise source in the centrifugal pump is mainly derived from the inner surface of the volute and the surface of the blade that strongly interferes with the medium. When the impeller rotates, the flow field can be approximated as a hydraulic near field, while the solid in the near water field acts as an additional effect of noise source. Its existence will interfere in noise distribution of the initial sound source. The sound energy emitted by the sound source is affected by the velocity and pressure strength of the medium, so the propagation of the secondary sound source can exceed the initial noise source [1]. Therefore, when the centrifugal pump is operating, the wake flow field of the blade is a relatively weak initial source. The volute tongue becomes a strong secondary noise source after the initial source propagates through the complex flow field.

The boundary element method (BEM) and the finite element method (FEM) solve acoustic problems in low frequency bands based on wave equations. The pressure pulsation on the surface of the volute is used as the acoustic boundary condition after the Fast Fourier Transform. The inlet and outlet of the model are defined as the full sound absorption property, and the shell is set as the total reflection wall. Direct boundary element method (DFEM) is used to solve this problem.

3. Geometric Model and Numerical Calculation Method

3.1 Model and flow field calculation method

This passage takes single-stage single-suction centrifugal pump as the research object, and its main structural parameters are shown in Table 1. The fluid domain of the centrifugal pump is modelled by three-dimensional software, as shown in Fig. 1. The fluid domain of the model is divided into volute, impeller, front and rear chamber, volute clearance and inlet and outlet section. s1 and s2 are sound pressure monitoring point of centrifugal pump.

Taken the complexity of the shape of the model structure into account, the model is divided by the non-structural mesh with good adaptability, and the complex structure is encrypted. The fluid domain model is shown in Fig. 2(b). The grid-independent inspection finally determines that the mesh of the entire fluid domain is 2.6673E+06, in which the impeller region is 7.435E+05; the volute region is 6.523E+05, and the rest of the region is about 1.27E+06.

The RNG k-ε model and the SIMPLEC algorithm are used to calculate the full flow field of the centrifugal pump. The inlet and outlet are respectively set as the

Table 1 Main structure parameters of centrifugal pump

Physical quantity	Parameter	Value
flow rate/$m^3 \cdot h^{-1}$	Q_v	12.5
head/m	H	20
rotational speed/$r \cdot min^{-1}$	N	2900
inlet diameter/mm	D_1	50
outlet diameter/mm	D_2	130
outlet width/mm	b_2	6
blade number	Z	5

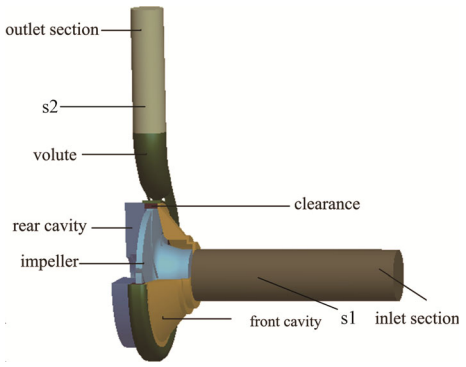

Fig. 1 Centrifugal pump three-dimensional fluid calculation domain

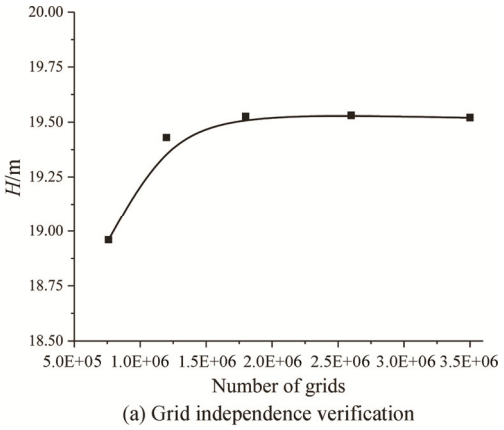

(a) Grid independence verification

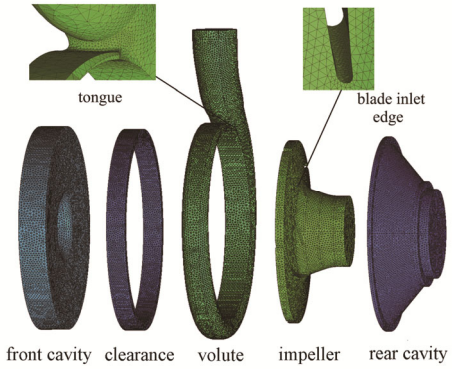

(b) Fluid calculation domain mesh

Fig. 2 Grid section

pressure inlet and the mass outlet, and the solid wall is no slip. The interface between the impeller and the pump body is the frozen rotor model. The convergence accuracy of the residual is 1.0E–05. The unsteady calculation is performed on the basis of steady calculation. The interface between the impeller and the volute is set as the transient dynamic and static interface, and a time step is equal to the time taken for the impeller to turn 3°. The time step is 1.724E–04. When the flow field shows a stable periodic change, extract the pressure pulsation of the volute and the impeller surface and save 4 cycles as the basis for the next calculation of the sound field.

The main factor affecting the noise of the inner sound field is the dynamic and static interference in the flow field, vortex and so on. In order to observe the changes in the flow field, take the section of the volute as a reference. Starting from the tongue, set a monitoring point (P_0–P_8) in each axis section (a total of 8 axis sections, from I to VIII, the angle between adjacent two axis sections is 45°) and set three monitoring points P_9–P_{11} at the outlet. The arrangement of the monitoring points is shown in Fig. 3.

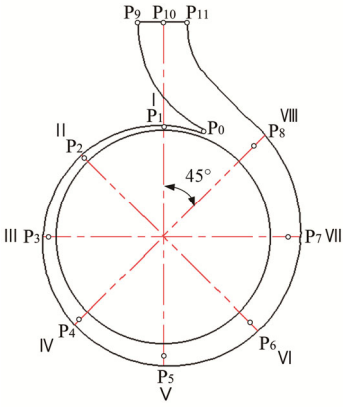

Fig. 3 Monitoring point location

3.2 Validation of the calculation model

Fig. 4 shows the model pump test bench. The test is conducted at the Fluid Machinery System Research Center of Lanzhou University of Technology. The relative flow is the ratio of the actual flow Q to the design flow Q_v. Five test conditions are carried out for the model pump. The test conditions are $0.6Q_v$, $0.8Q_v$, $1.0Q_v$, $1.2Q_v$ and $1.4Q_v$. Fig. 5(a) is the comparison curve between the experimental head and the calculated head. It can be seen from the figure that the two curves are consistent. Under small flow conditions, the head has a large difference and the maximum relative error is 4.7%. As the flow rate increases, the error between the two becomes smaller. The calculated value of the head in the optimal working condition and the large flow condition is in good agreement with the experimental value. Fig. 5(b) shows the comparison between the sound field exit monitoring point and the simulated value in the model pump. It can be seen from the figure that the simulated value is generally lower than the test value, which is mainly caused by the motor work and the liquid storage tank interference to the test, but the two trends are basically consistent, especially the blade passing frequency and the frequency multiplication coincide well. Therefore, the results of this model calculation can be used as the data source for sound field calculations.

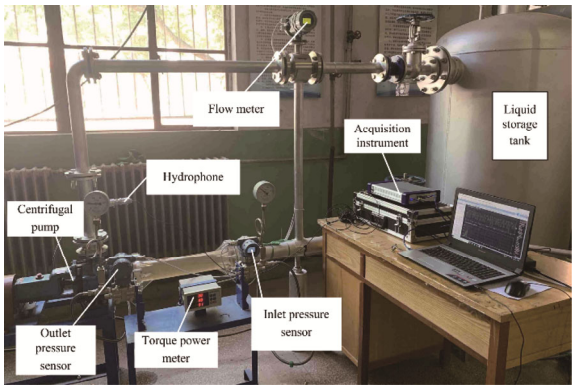

Fig. 4 Test system

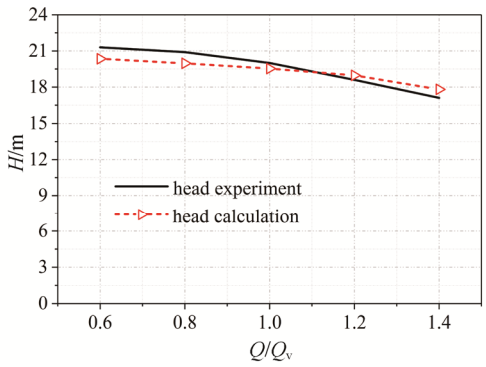

(a) Characteristic curves of model pump

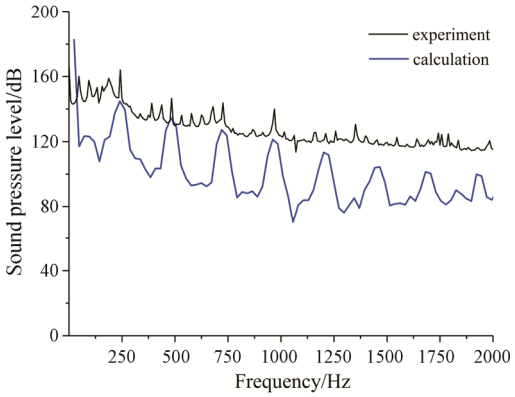

(b) Internal sound field verification

Fig. 5 Verification of Model Pump

4. Numerical Calculation Results and Analysis

4.1 Pressure pulsation analysis

Unsteady calculations are carried out for $0.6Q_v$, $0.8Q_v$, $1.0Q_v$, $1.2Q_v$, $1.4Q_v$, and four cycles are taken to analyze the pressure pulsation when the flow field showed a stable periodic change. The blade passing frequency can be calculated by Eq. (5).

$$f = \frac{nZ}{60} \tag{5}$$

where n is the rotational speed; Z is the number of blades. Z is 1 when calculating the shaft frequency. The shaft frequency of the research object is determined to be 48.3 Hz, and the blade passing frequency is 241.6 Hz. In order to eliminate the influence of the static pressure of the monitoring point itself on the pressure pulsation, the pressure pulsation coefficient C_P is introduced as the ordinate of the frequency domain diagram.

$$C_P = \frac{P - \overline{P}}{\frac{1}{2}\rho u_2^2} \tag{6}$$

where P is the pressure at the monitoring point at a certain time; $\overline{P}$ is the average pressure of the monitoring point of one revolution of the impeller. And u_2 is the peripheral speed of the impeller outlet; ρ is the density of the medium.

Fig. 6 shows the pressure fluctuation characteristics of each monitoring point under five working conditions. By processing the pressure pulsations based on the Fast Fourier Transform, it can be seen from Fig. 6 that the peak value of pressure pulsation mainly occurs in the shaft frequency, blade passing frequency and multiple of the blade passing frequency. The pressure pulsation peak of blade passing frequency is the largest. As the frequency increases, the pressure pulsation peak appears to be greatly attenuated. It indicates that the blade passing frequency is the main frequency of pressure pulsation inside the volute. Under each monitoring point, P_0, P_1, P_2 and the outlet monitoring point P_9–P_{11} have the strongest pressure pulsation. The reason is that the fluid is pumped out from the high-speed rotating blade passage, continuously impacting the tongue and forming an unstable flow at the narrow I and II sections. As the area of flow passage becomes wider and begins to move away from the tongue, the flow in other sections begins to stabilize. At this time, the change of pressure pulsation is very small, but the pressure pulsation increases after the VIII section. This is due to the fact that the unstable flow at the tongue has a certain influence on the vicinity of the volute outlet, resulting in an increase in the pressure pulsation peak at the outlet. It can be seen that the vicinity of the tongue is the most important area of rotor-stator interaction between the impeller and the volute. The degree of pressure pulsation varies under different working conditions at the same monitoring point. It can be seen from Fig. 6 that compared with other working conditions, the pressure fluctuation of the design condition is lower. The pulsation peak attenuates quickly in the shaft frequency, and the pulsation peak is mainly concentrated in the blade passing frequency and the multiple frequency. Under the low flow conditions, the outlet pressure is strong. The internal complex flow change and the randomness of vortice and turbulence causes flow separation and backflow in the centrifugal pump. And a strong vortex is generated in the shear layer between the mainstream and the reflow, which enhances the broadband pressure pulsation under the blade passing frequency. Under the high flow conditions, the pressure pulsation near the tongue is strengthened. This is because the increase of the flow rate makes the tail of the blade more likely to reveal boundary layer separation, and the formation of strong blade jet and wake effect lead to an increase in pressure pulsation. In general, the blade passing frequency is the main frequency of the pulsating peak, and the rotor-stator interaction between the tongue and the impeller is the main cause of the pressure pulsation.

Fig. 7 is a pressure contour of the blade relative to the tongue position at different times. It can be seen from the figure that the back of the blade outlet is kept at a low pressure. When the blade is turned to the tongue, the wake formed by the blade hits the head of the tongue, which causes the pressure near the head of the tongue to rise. And the flow of the outlet is the largest at this time. For this reason, the local pressure in the outlet section decreases. As the blade begins to move away from the tongue, the fluid is blocked by the tongue and the outlet flow reduces, which in turn increases the pressure to the outlet. The rotation of the blade also affects the significant change in pressure near the volute first section. This is because the blade-driven wake forms a “jet” in the narrow I section, and interacts with the trailing jet of the blade, causing a sudden increase in the flow velocity and a sudden drop in pressure. The pressure between the volute tongue and the outlet is constantly changing as the blade keeps sweeping the tongue.

In order to study the variation law of pressure pulsation near the volute tongue, three monitoring points are arranged near the tongue as shown in Fig. 8. OC is the line connecting the exit point of the blade profile line to the center of the base circle, defined as the position of the initial moment of the blade. OC' is the position where the blade rotates by a blade rotation angle of 72°, and it is recorded as T_{blade} at this time. Observe the physical changes of the three points D, E, and F. Fig. 9 shows the

tangential velocity, radial velocity and static pressure distribution of monitoring points D, E, F near the tongue in a blade rotation angle. When the blade passes the monitoring point D at $0.1T_{blade}$, the pressure will drop to the lowest. The radial velocity at point D decreases, and the tangential velocity increases. This is caused by the jet formed by the pressure gradient in the wake zone and the jet zone. As shown in Fig. 10, there is a distinct wake jet region at the tail of the blade. When the blade turns to the tongue at $0.5T_{blade}$, the pressure at point E will drop. When the blade is at $0.7T_{blade}$, the pressure will reduce and the tangential velocity will be high. This is because the blade drives the liquid to form a jet in a narrow flow channel, resulting in a higher tangential velocity. On the

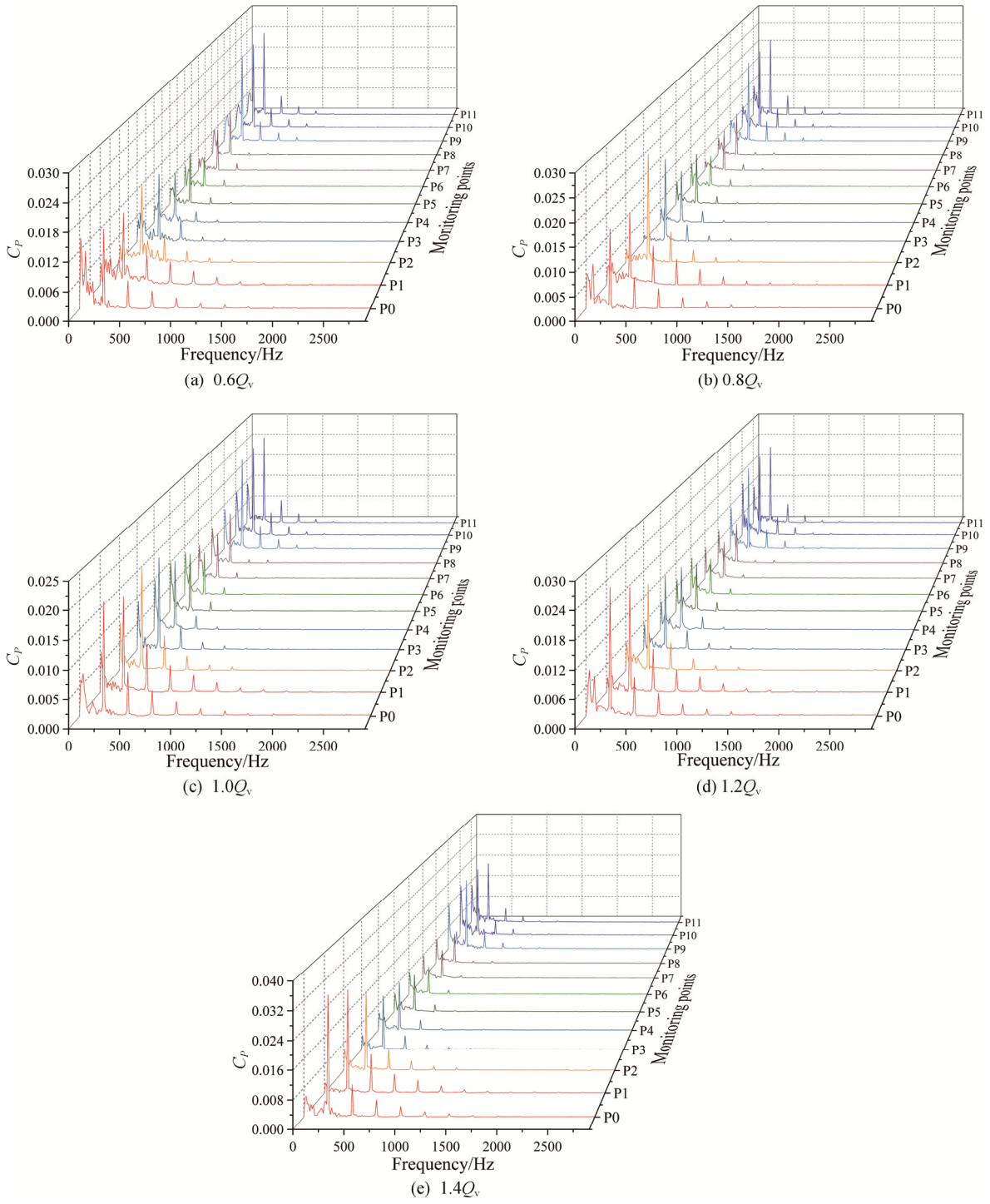

Fig. 6 Monitoring point pressure pulsation frequency domain curve

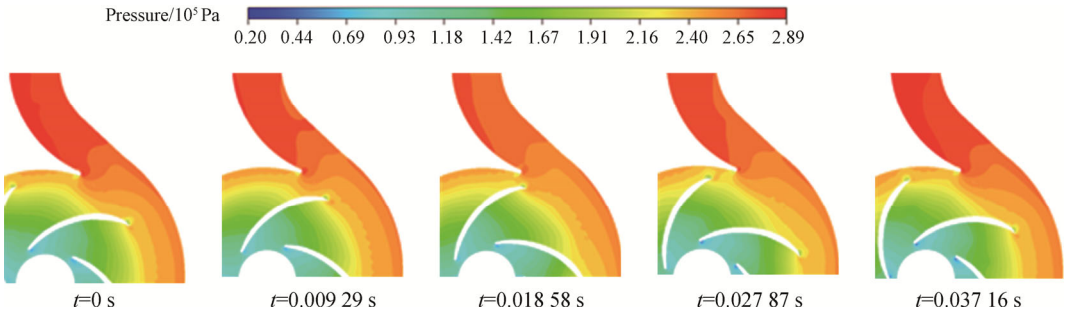

Fig. 7 Static pressure of the blade relative to the tongue at different times

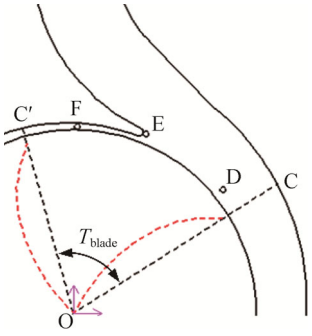

Fig. 8 Tongue monitoring point

whole, the pressure in the area of the blade outlet will drop significantly because of the blade acting as a hindrance to the fluid and there is a pressure gradient between the pressure surface and the suction surface of the blade to make the blade outlet have a higher tangential velocity, resulting in a decrease in the pressure at the blade outlet.

4.2 Sound field calculation results and analysis

The acoustic field calculation of the internal flow field is based on the unsteady flow field data. The main noise source in the pump is the volute surface dipole. In this study, the pressure pulsation of the volute surface is extracted as a dipole noise source. At the same time, the boundary element mesh is divided, considering the reflection, diffraction, refraction and other effects of the sound and the correspondence between the grid element size and the calculation frequency. Assuming that 6 cell grids are required in the minimum wavelength, the following formula is satisfied.

$$L \le \frac{c}{6 f_{\max}} \tag{7}$$

L represents the grid scale, and c represents the propagation velocity of the sound in the medium. And $f_{\max}$ represents the highest calculation frequency. The medium in this study is water, and the sound is at a speed of 1500 m/s. The density is 1000 kg/m^3. The maximum frequency that can be calculated by the boundary element mesh is 7000 Hz, and the actual required calculation frequency is completely in accordance with the

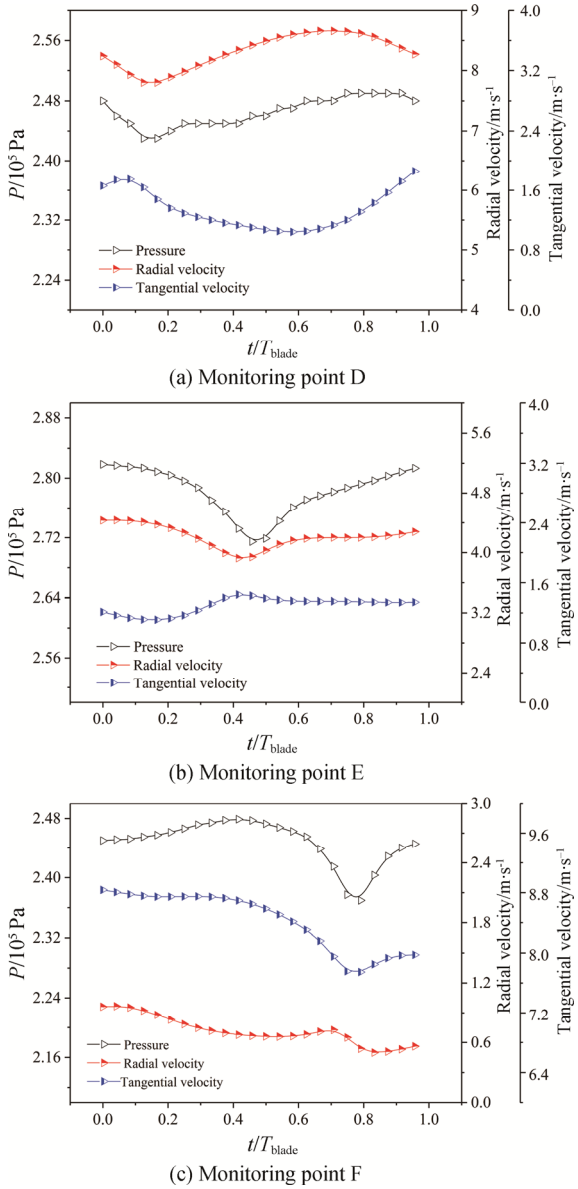

(a) Monitoring point D

(b) Monitoring point E

(c) Monitoring point F

Fig. 9 Pressure, radial velocity and tangential velocity distribution near a tongue in a blade rotation angle

requirements. Set the inlet and outlet of the model pump to the sound absorption property, and set a field point s_1, s_2 in the inlet and outlet of the pump for monitoring.

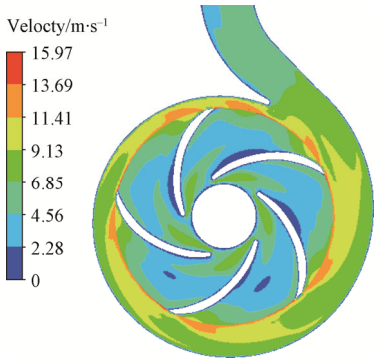

Fig. 10 Velocity cloud map of the volute under design flow

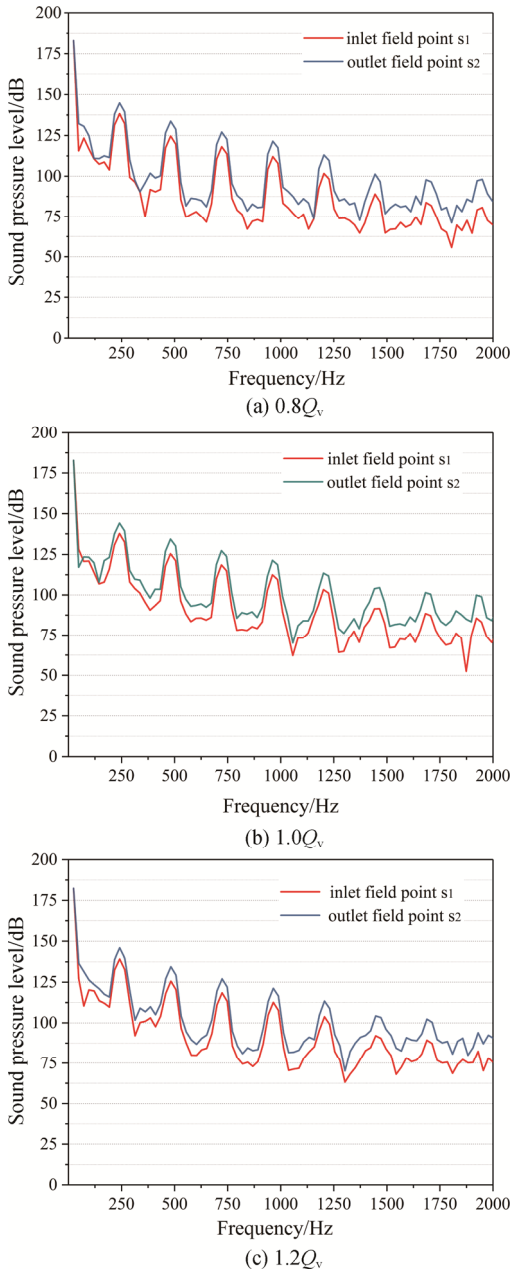

Fig. 11 Sound pressure level spectrum of field points s_1 and s_2 under different flow rates

Fig. 11 shows the sound pressure level spectrum of the inlet and outlet field point at 0.8Q_v, 1.0Q_v, and 1.2Q_v. It can be seen from the figure that the sound pressure level at the outlet is significantly larger than that of the inlet. This shows that the effect of using the dipole as the sound source on pump outlet is greater than that of the inlet. The sound pressure level frequency of the inlet and outlet fields is broadband, but peaks at the blade passing frequency and the multiple frequency and there is obvious discreteness. This indicates that the rotor-stator interaction between the blade and the tongue is the main factor inducing noise. The maximum sound pressure level under the blade passing frequency is the lowest at the design flow rate. The sound pressure levels at other deviations from the design flow rate are larger than the design flow rate. This means that the pump needs to operate at the design flow to reduce noise.

In the numerical simulation of the inner sound field, 15 monitoring field points are set according to the spiral line with reference to the base circle, and the starting point of the eighth section is 0° as shown in Fig. 12. Fig. 13 is the distribution of the sound pressure level of the

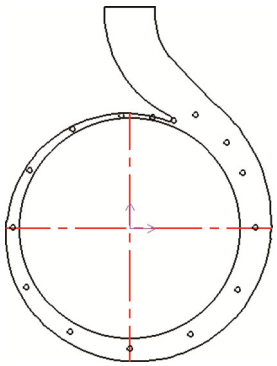

Fig. 12 Sound pressure monitoring point distribution

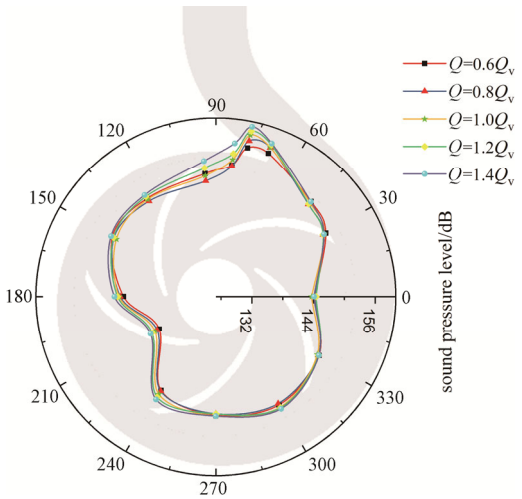

Fig. 13 Sound pressure picture of monitoring points of different flow volutes

monitoring point under various flow conditions. Under the five conditions, the inner sound field is characterized by dipole characteristics. The difference in sound pressure level is mainly distributed in the tongue and the third section. There are obvious peaks in the vicinity of the tongue. This shows that the interaction of the blade and the tongue has a significant effect on the internal flow field noise under five different flow conditions. Due to the narrow flowing passage of the third section, the disturbance near the tongue has a great influence on it, so it shows a large difference in sound pressure level. As the area of passage expands and moves away from the tongue, the difference in sound pressure level of other sections changes little. When the design flow is deviated, the absolute velocity of the impeller increases at the outlet and the vortex in the flow passage significantly increases compared with the previous one. The turbulence in the large flow conditions intensifies and the fluid is more prone to show flow separation near the boundary layer at the exit of the impeller under the action of the adverse pressure gradient. It causes the jet-wake at the outlet of the impeller to be aggravated, and the discrete noise at this time is large.

4.3 Sound field distribution

Fig. 14 is a contour of sound pressure level of different frequencies of APF (shaft frequency), BPF (blade passing frequency), and 2BPF (double balde passing frequency) under design conditions. It can be seen from the figure that the sound pressure level of the blade passing frequency has the highest intensity, and the sound pressure level intensity distribution of other frequencies shows significant attenuation. Therefore, the blade passing frequency can be considered as the main frequency of noise. At different frequencies, the sound pressure level of the outlet is always greater than that of the inlet. The area with the maximum sound pressure level is mainly concentrated near the tongue and the outlet of the volute, and the sound pressure level gradient in this area is obvious, further indicating that the rotor-stator interaction near the tongue has a strong influence on the noise.

Fig. 15 is a model of the sound pressure level distribution under different flow conditions at the blade passing frequency. It can be seen from the figure that the tongue and volute outlet are the main concentrated areas of the maximum sound pressure level. It can be seen from the figure that the tongue is the main source of noise. The maximum sound pressure level under the off-design conditions is larger than the design condition (as seen from Fig. 11), and the sound pressure level near the second section of the volute under the off-design condition is obviously higher than that under the design condition. This difference is more pronounced as the flow deviates from the design flow. This is due to the fact that the geometry of the volute and the tongue are unchanged when the design flow is deviated, but the change of flow rate causes a large change in the direction and velocity of the flow at the impeller outlet. Inevitably, the vortex and liquid flow in the volute, especially near the tongue, hit the wall, causing the jet-wake effect to make the flow of the internal flow field complex. It results in an increase in the sound pressure level. The change in flow rate will affect the hydrodynamic noise of the sound field greatly.

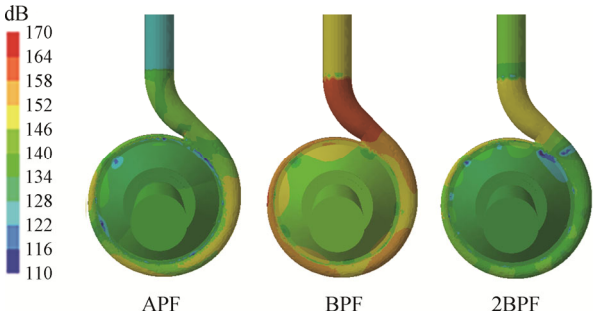

Fig. 14 Sound pressure levels at different frequency under the design flow

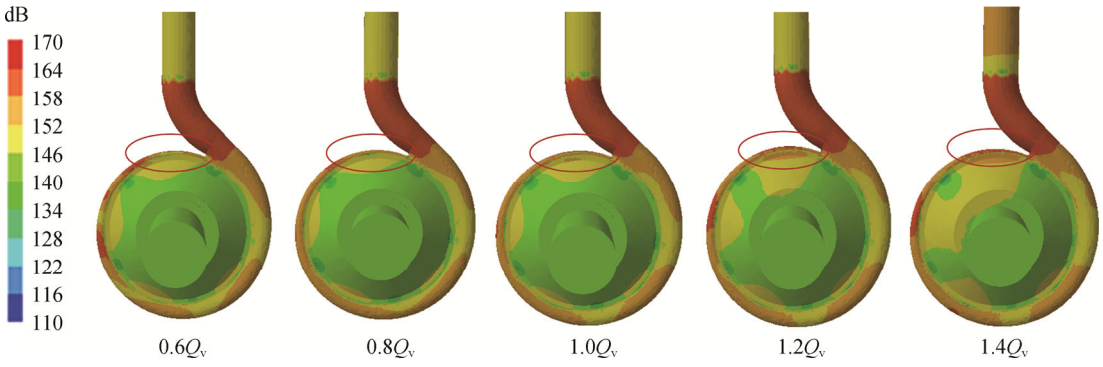

Fig. 15 Sound pressure levels in various working conditions under blade passing frequency

5. Conclusion

(1) The rotor-stator interaction between the volute tongue and the impeller is the main cause of the drastic change of the pressure pulsation peak in the volute. The pressure pulsation at the tongue is the highest under the design flow and large flow conditions, and the volute outlet is the second. The small flow condition shows that the outlet pressure pulsation is higher than the tongue, and the pulsation peak under different working conditions is mainly concentrated in the blade passing frequency and the peak at the blade passing frequency and multiple frequency is the highest. The pressure pulsation in the tongue area of different working conditions is the lowest under the design condition.

(2) The turbulent pressure pulsation has a certain correlation with the internal flow field noise, and the sound pressure level in the region with large turbulent pressure pulsation peak is also large. They have a positive correlation.

(3) The jet-wake causes low pressure at the back of the blade outlet. When the blade sweeps the tongue, the jet will cause a higher tangential velocity and a lower radial velocity in the blade outlet, and the pressure near the tongue is always higher than other region.

(4) The sound field distribution in the volute exhibits dipole characteristics, and the sound pressure level gradient near the tongue is large. The tongue is the main noise source. Under the different frequency, the sound pressure level under the blade passing frequency is the highest, and the sound pressure level in the outlet section is larger than that in the inlet. The flow rate is the main factor affecting the noise of the internal sound field. And the maximum sound pressure level under the design working condition is the lowest compared with other working conditions.

Acknowledgement

This work is supported by the National Natural Science Foundation of China (No. 51469013).

References

[1] Yuan S.Q., Yuan J.P., Pei G., Centrifugal pump internal flow and operation energy saving. Science press, Beijing, China, 2016. (in Chinese)

[2] Liu H.L., Tan M.G., Modern design methods for centrifugal pumps. China machine press, Beijing, China, 2013. (in Chinese)

[3] Bosioc A.I., Muntean S., Draghici I., Hydrodynamic analysis of the flow in an axial rotor and impeller for large storage Pump. IOP Conference Series Earth and Environmental Science, 2016, 49(3): 032016.

[4] Chalghoum I., Kanfoudi H., Elaoud S., Numerical modeling of the flow inside a centrifugal pump: influence of impeller–volute interaction on velocity and pressure fields. Arabian Journal for Science & Engineering, 2016, 41(11): 1–14.

[5] Cai J., Jie P., Guzzomi A., The flow field in a centrifugal pump with a large tongue gap and back blades. Journal of Mechanical Science & Technology, 2014, 28(11): 4455–4464.

[6] Zhou Z.F., Chen S.S., He Z.N., PIV orthogonal measurement for internal flow pattern within centrifugal pump impeller. Journal of Hua-zhong University of Science and Technology Natural Science Edition, 2016, 129: 012013. (in Chinese)

[7] Biao Q., Bo Y.U., Wei L., Measurement of cavitation noise in centrifugal pump. Journal of Drainage and Irrigation Machinery Engineering, 2016. (in Chinese)

[8] Liu H.L., Dai H.W, Ding J., Numerical and experimental studies of hydraulic noise induced by surface dipole sources in a centrifugal pump. Journal of Hydrodynamics, Ser. B, 2016, 28(1): 43–51. (in Chinese)

[9] Liu H., Li Y., Wang K., Study on radiated noise characteristics of multistage centrifugal pump under fluid excitation. Journal of Huazhong University of Science & Technology, 2017, 45(11): 92–97. (in Chinese)

[10] Zheng L.L., Dou H.S., Chen X.P., Numerical simulation of pressure fluctuation around the tongue region in a centrifugal pump. Iop Conference Series: Earth & Environmental Science. IOP Conference Series: Earth and Environmental Science, 2016.

[11] Liu H.L., Ding J., Wang Y., Numerical simulation of hydrodynamic noise in centrifugal pump based on LE. Journal of Mechanical Engineering, 2013, 49(18): 177–183. (in Chinese)

[12] Dong L., Dai C., Kong F., Impact of blade outlet angle on acoustic of centrifugal pump as turbine. Transactions of the Chinese Society of Agricultural Engineering, 2015, 31(06): 69–75. (in Chinese)

[13] Dong P.X., Gao M., Guan H.J., Numerical simulation for variation law of volute radiated noise in centrifugal pumps under variable rotating speed. Journal of Vibration and Shock, 2017, 36(13): 128–133. (in Chinese)

[14] Wang Y., Liu H.L., Liu D.X., Effects of vane wrap angle on flow induced vibration and noise of centrifugal pumps. Transactions of the Chinese Society of Agricultural Engineering, 2013, 29(01): 72–77. (in Chinese)

[15] Dai C., Dong L., Kong F.Y., Noise reduction by actively leaning blades in centrifugal pump as turbine. Journal of Shanghai Jiaotong University, 2016, 50(4): 575–582. (in Chinese)

[16] Dai C., Kong F.Y., Dong L., Noise reduction by

counter-leaning blade and tongue for centrifugal pump as turbine. Journal of Vibration Engineering, 2016, 29(4): 623–630. (in Chinese)

[17] Zhang J.F., Jia J., Hu R.X., Flow noise of pipeline pump and bionic sound optimization. Transactions of the Chinese Society for Agricultural Machinery, 2018(9): 138–145. (in Chinese)

[18] Mao H., Wang Y., Lin P., Influence of tip end-plate on noise of small axial fan. Journal of Thermal Science, 2017, 26(1): 30–37.

[19] Wu G., Lu Z., Xu X., Numerical investigation of aeroacoustics damping performance of a Helmholtz resonator: Effects of geometry, grazing and bias flow. Aerospace Science and Technology, 2019, 1(86): 191–203.

[20] Papaxanthos N., Perrey-Debain E., Bennouna S., Pressure-based integral formulations of Lighthill–Curle's analogy for internal aeroacoustics at low Mach numbers. Journal of Sound & Vibration, 2017, 393: 176–186.

[21] Layton W., Novotný A., On Lighthill's Acoustic analogy for low mach number flows. Advances in Mathematical Fluid Mechanics, 2016: 247–279.

[22] Zhang N., Wang X., Xie H., Research on numerical simulation approach for flow induced noise and the influence of the acoustic integral surface. Journal of Ship Mechanics, 2016, 20(7): 892–908. (in Chinese)